List of Figures

A Global, Single-Input-Multi-Output (SIMO) Implementation of The Algorithm of Mode Isolation and Application to Analytical and Experimental Data

Matthew S. Allen* and Jerry H. Ginsberg

G. W. Woodruff School of Mechanical Engineering

Georgia Institute of Technology

Atlanta, GA 30332-0405

May 20, 2005

*Corresponding author. *E-mail:* msalle@sandia.gov, *Fax:* (404) 894-8496

ABSTRACT

This work presents a global, single-input-multi-output (SIMO) extension of the Algorithm of Mode Isolation (AMI) in which the frequency response functions (FRFs) from all measurement points are considered simultaneously, resulting in global estimates for natural frequencies and damping ratios, and consistent mode vectors. This allows a large number of response points to be processed quickly and with minimal user interaction and makes determining the number of modes active in a frequency band easier than with a SISO algorithm. To achieve a global, SIMO AMI algorithm, a fast new linear-least-squares, frequency domain, global, SIMO (or common denominator MIMO), multi-degree of freedom (MDOF) fitting algorithm, similar to the LSCF algorithm is derived and implemented in AMI. This implementation of AMI is then compared with the Stochastic Subspace Identification algorithm (SSI) on noise contaminated analytical data. Some practical issues in applying the SSI algorithm are discussed. Monte Carlo simulations are used to compare the natural frequencies and damping ratios found by AMI and SSI for noise contaminated, synthetic data for a frame structure. The results for the analytical structure also illustrate the difficulty in processing data from a structure having modes with a large range of decay rates. Finally, application to data from the Z24 highway bridge in Switzerland demonstrates the speed and flexibility of the algorithm, and validates its performance on experimental data.

KEYWORDS: Civil structures, MIA, Composite Nyquist

NOMENCLATURE

$H_{jP}(\omega)$	FRF for displacement j due to excitation P
H_{c}	Composite FRF
H_{cn}	Condensed FRF (Nyquist Plots)
$\{A_{P,r}\}$	Modal residue vector for the rth mode driven at P
λ_r	rth eigenvalue
$\{\phi_r\}$	displacement portion of rth state-space mode vector (Normalized)
ω_r	rth natural frequency
ζ_r	rth modal damping ratio
$\{q\}$	Generalized coordinates
w	Transverse displacement
θ	Torsional rotation
ω	Drive frequency
N_o	Number of outputs
α	Peak selection parameter

1 Introduction

As applications of experimental modal analysis (EMA) expand, the need for accurate algorithms capable of handling large data sets with low signal to noise ratios is apparent. In order to accurately characterize the spatial nature of the modes of a vibrating structure, many measurements are often made. For frequency domain algorithms these measurements yield frequency response functions (FRFs). In principle, each FRF contains the information needed to estimate the eigenvalues or natural frequencies and modal damping ratios of the system. However, one would expect that global single-input-multi-output (SIMO) and multi-input-multi-output (MIMO) algorithms, by simultaneously matching redundant information, should result in more accurate estimation of natural frequencies and damping ratios

and consistent mode shapes. Furthermore, global algorithms can reduce user interaction and data-processing time.

The objectives in experimental modal analysis differ from those in general system identification, in that the goal is meaningful modes of vibration, rather than matching of input and output data. Virtually all MDOF identification algorithms return a number of computational modes intermixed with the true system modes. Determination of the model order that gives the most accurate modal parameters for the true system modes, and distinguishing true system modes from computational ones, are critical aspects of EMA. Allemang [1] stated: "The estimation of an appropriate model order is the most important problem encountered in modal parameter estimation." In [2] Allemang also noted that model order determination comprises much of the user interaction involved in experimental modal analysis.

Error charts [1] [2] or plots of singular values (as in ERA or SSI, for example [3],[4],[5]) may suggest a model order that results in modal parameters that are sufficiently accurate for many purposes, though optimality has not been studied. Careful inspection of a stabilization diagram will give an indication of the magnitude of variance from one model order to the next, but bias errors that are stable relative to model order are more difficult to detect. Common practices for computing stabilization diagrams in a time efficient way may not reveal bias errors, as shown by the authors [24] for the SSI algorithm.

The stabilization diagram is also the primary tool for distinguishing computational modes from true system modes. There are a number of tools available to assist in this. Goethals and De Moor [6] found that energy could be used to distinguish many of the spurious modes. Verboven *et al* [7] used pole characteristics as well as properties of the stabilization diagram, such as the variation in a pole's frequency from one model order to the next, to detect spurious modes. Marchesiello *et al.* [8] created a histogram or probability density function from a number of stabilization diagrams in order to show where modes were most likely to reside. While these represent substantial aid, an absolute criterion for detecting spurious modes for a general problem has not been developed. In some frequency ranges, stable modes may not be visible [9].

The Algorithm of Mode Isolation (AMI) operates in a manner that can obviate the need for a stabilization diagram. This work presents a global, SIMO extension to AMI in which FRFs for all response points are processed simultaneously. The resulting AMI-SIMO algorithm is computationally efficient, and requires minimal user interaction to process data sets for many measurement points. As with previous versions of AMI, the number

of modes situated in the frequency band of interest is determined along with modal parameters. AMI begins by identifying modes one at a time, and then subtracting their contribution from the data. In this process the importance of each mode to the fit is clearly visible. The number of true modes in the data set is taken to be the number of modes that must be fit to the data to reduce it to noise. An iterative procedure then refines the initial estimate. The resulting MDOF fit does not introduce any spurious or computational modes. Because modes are identified one at a time, only a single degree of freedom fit is needed, which makes the algorithm computationally efficient, with small workspace requirements. Previous comparisons of AMI to some standard MDOF algorithms [10], [11] have shown that AMI performs favorably when applied to synthetic data for a few prototypical analytical systems.

The primary new feature of the present work is its implementation of a refined technique for fitting individual modes, in which all FRF data from a SIMO/MISO test are used concurrently. In [24] the authors presented a SIMO-SDOF fitting algorithm, achieved by expanding the data set and vectorizing the SDOF algorithm in [15]. The SIMO-SDOF algorithm in [24] was found to be similar to a continuous time implementation of the LSCF algorithm presented by Guillaume *et al* in [16] and [17], though Guillaume *et al* implemented two features that are attractive for application in AMI. First, they included an extra numerator term in the rational expression of the transfer function. This allows for modeling out of band effects, as described by [25]. Second, Guillaume *et al* formed the normal equations for the least squares problem directly, resulting in a fast, memory saving implementation. The algorithm presented herein incorporates both of these features while following the derivation in [24] rather than that presented by Guillaume *et al*. This change in the derivation, coupled with the restriction that the weighting function be the same for all measurement points, allows for further computational savings.

The performance of AMI, using this new SIMO fitting algorithm, is demonstrated on noise contaminated analytical response data for a frame structure. For comparison purposes, the output-only Stochastic Subspace Identification Algorithm (SSI) is also applied to the data and the results are compared. The use of analytical data allows for the performance of the algorithms to be compared using a system for which the true modal parameters are known. The disadvantage of using analytical data lies in the fact that the noise model used may not be realistic for all experiments. The performance of the proposed SIMO-AMI algorithm is also demonstrated here on experimentally measured, drop test data for the Z24 Highway bridge in Switzerland (see [8], [33], [34], [36] and [37].)

This data is inherently SIMO because the exciter was dropped at only one location, and thus presents a good test set for SIMO-AMI. Most of the researchers cited found that better results were obtained when processing the MIMO shaker-driven data set taken from the bridge, thus affirming the difficulty presented by this data set.

The first section of this paper gives a brief description of the Algorithm of Mode Isolation. In the next section a Global, SIMO, multi-degree of freedom (MDOF) fitting algorithm is presented for use in AMI. The third section presents the application of AMI to noise contaminated analytical data for a frame structure, and compares the results to those derived from the Stochastic Subspace Algorithm. The fourth section presents the application of AMI to data from the Z24 highway bridge. Finally, some conclusions are presented.

2 The Algorithm of Mode Isolation

The general concept of mode isolation was first suggested by Kirshenboim [12] and seems to have been implemented as part of the Modent package [13]. The first detailed investigation of the methodology was presented much later by Drexel and Ginsberg [10], in which it was dubbed the Mode Isolation Algorithm (MIA), and then subsequently the Algorithm of Mode Isolation (AMI). While the references to the methodology are sparse in the literature, a few researchers have reported trying similar procedures in communications with the authors. Recently, Yin and Duhamel [14] reported using a similar technique, though they used finite difference formulas to identify the modal parameters, whereas AMI uses a least-squares fit. Improvements to the AMI algorithm presented originally by Drexel and Ginsberg and results of test problems are documented in [11], [15], [18], [19], [20], [21] and [22]. AMI is based upon the recognition that the FRF data to be fit is a superposition of individual modal contributions. It identifies each mode sequentially, and then uses the identified mode's parameters to subtract its contribution from the FRF data. Once all of the modes have been subtracted, only noise remains, thereby identifying the model order as the number of modes subtracted before the data is reduced to noise. An iterative procedure is then used to refine the initial estimate in order to account for overlapping contributions of adjacent modes. The algorithm also provides a self-correcting check that the initial identification of the number of contributory modes is correct.

The procedure will be described briefly here. The discussion will focus on the present global, SIMO implementation. Differences between this and the prior SISO implementation will be highlighted. The data analyzed in AMI consists of the frequency response of all measurement degrees of freedom (DOF) to a harmonic

force at the Pth measurement DOF. (By reciprocity this is equivalent to the response of the Pth DOF to a force applied to each measurement DOF sequentially.) It is assumed that the system dynamics can be represented by the familiar second order matrix differential equation

$$[M]\{\ddot{q}\} + [C]\{\dot{q}\} + [K]\{q\} = \{F\} \tag{1}$$

where $\{q\}$, $[M]$, $[C]$, and $[K]$ are the generalized coordinate vector, and symmetric mass, damping and stiffness matrices respectively each of dimensions $N \times N$. The force vector $\{F\}$ is zero everywhere except the Pth generalized coordinate (or drive point) for a SIMO experiment. The frequency response function $\{H_P(\omega)\}$ is the ratio of the complex response amplitude of each generalized displacement to the drive force amplitude. It is related to the state space modal properties by

$$\{H_P(\omega)\} = \sum_{r=1}^{N} \left[\frac{\{A_{P,r}\}}{i\omega - \lambda_r} + \frac{\{A_{P,r}^*\}}{i\omega - \lambda_r^*} \right] \tag{2}$$

$$\{A_{P,r}\} = \lambda_r \{\phi_r\} \phi_{Pr}$$

where λ_r and $\{\phi_r\}$ are the complex eigenvalue and the displacement portion of the complex normalized eigenvector of the rth mode of vibration and $()^*$ denotes a complex conjugate. The notation ϕ_{Pr} signifies the Pth element of the rth mode vector, or the Prth element of the displacement portion of the modal matrix, and $\{A_{P,r}\}$ is the Pth column of the residue matrix for mode r. The eigenvalue is related to the natural frequency ω_r and damping ratio ζ_r by $\lambda_r = -\zeta_r \omega_r + \omega_r \left(1 - \zeta_r^2\right)^{1/2}$. See [22] or [23] for a more detailed discussion of the state space eigenvalue problem and mode vector normalization.

2.1 Subtraction Phase

AMI begins with the subtraction phase, in which modes are subtracted from the experimental data one at a time. The algorithm starts by considering the dominant mode, located as the highest peak of the composite FRF, where the composite FRF $H_c(\omega)$ is defined as the average of the magnitude of the FRFs for all response points,

$$H_c(\omega) = \frac{1}{N_o} \sum_{j=1}^{N_o} |H_{jP}(\omega)| \tag{3}$$

with N_o being the number FRFs. If corresponding peaks in the FRFs for different response points have vastly different amplitudes, it may be advisable to scale the FRFs before forming the composite, though care must be taken so as to avoid amplifying the effect of measurement noise. The previous SISO implementation of AMI operated successively on a single FRF, and thus did not consider a composite FRF.

The FRF data sets for all measurement points in the vicinity of the peak composite FRF are sent to a SIMO, SDOF fitting algorithm (described subsequently) that returns the eigenvalue and mode vector that best fit the dominant mode to all FRFs. The number of data points around the peak that are fit is a compromise between averaging out noise (more points) and reducing the contribution of other modes (fewer points). Selection of the FRF points to be used in the fitting procedure is automated by selecting data such that

$$H_c(\omega) > \alpha * \max(H_c(\omega)) \tag{4}$$

where the peak selection parameter α defines the range of points used. For example, $\alpha = 0.707$ corresponds to using all points above the half-power points.

An FRF model for the fit mode is then constructed using eq. (2), and the fit mode is subtracted from all FRF data. This brings the mode having the next highest peak into dominance. That mode is then identified and its contribution subtracted from the FRF data. The process continues until the composite FRF shows no coherent peaks suggestive of the presence of additional modes. Presently, this condition is determined by visual inspection of the data, as will be illustrated by the examples in subsequent sections.

It should be noted that this subtraction procedure is not likely to yield good initial approximations of the modal parameters of groups of modes having repeated or almost repeated natural frequencies. A MIMO extension to AMI, which is required to correctly identify modes with repeated natural frequencies, is an area of current research. However, the SIMO algorithm has been found to work well for many systems with relatively close natural frequencies, as demonstrated by the examples in subsequent sections.

2.2 Mode Isolation Phase

Once all of the modes of the system have been approximated, the estimate for each mode is refined through an iterative procedure. This phase proceeds through the modes in the sequence of their dominance in the composite FRF. The contributions of all modes except for the one in focus are subtracted from each FRF data set. This leaves only the experimentally measured contribution of the mode in focus, as well as noise and any errors that may exist in the fit of the other modes. The mode in focus is then re-fit using the SIMO / SDOF fitting algorithm. At this point, the data essentially contains only one mode, so an SDOF fit yields an improved estimate of the current mode's parameters. Also, because the contributions of all other modes have presumably been removed from the data, the

fitting algorithm can now consider more data around the peak, further minimizing the effects of noise. Care should be taken however. Because of the limited resolution of sensors and data acquisition equipment, data very far from the peak may not be reliable. As a general rule, the criteria in eq. (4) with $\alpha = 0.5$, yields good results. Using Monte-Carlo simulations, Ginsberg *et al* found that this was optimum for a single FRF contaminated with random, white noise. However, for systems with heavily damped modes or very high noise, a larger α may be needed to assure that data very far from the peak is not included in the fit for the mode in focus.

The model is then updated with the modal parameters fitting the mode in focus, and the algorithm proceeds to the next mode. A cycle through all identified modes constitutes one iteration. Typically only a few iterations are required. Computations cease when convergence criteria for the eigenvalues and residues have been met.

2.3 SIMO Fitting Algorithm

The fitting algorithm used in SIMO-AMI is a SIMO extension of the algorithm presented in [15]. As noted in the introduction, this algorithm was found to be similar to the LSCF algorithm presented by Guillaume *et al* in [16]. In the derivation that follows, a number of features of the algorithm in [16] will be implemented, yet following the derivation presented originally by the authors in [24]. This leads to a frequency domain identification algorithm that is more computationally efficient than either of the algorithms in [16] or [24] when applied to data sets containing many output measurements. It is formulated to allow for an arbitrary number of extra numerator terms to be added to the fit. This algorithm is also similar to the Rational Fraction Polynomial (RFP) or Orthogonal Polynomial algorithm presented in [40], although a computationally efficient, memory saving implementation of the RFP algorithm has not been presented in the literature.

This algorithm and the others described previously can all be viewed as extensions of Levy's method, presented in [39]. A number of similar frequency domain parameter identification algorithms are discussed in Pintelon *et al* [30]. The basic idea in these methods is to express a SISO transfer function as a ratios of polynomials in $(i\omega)$ having real coefficients. For the SIMO FRF representation in eq.(2), this is done as follows:

$$\{H_P(\omega)\} = \frac{\sum_{k=1}^{N_n} \{B_k\} (i\omega)^k}{\sum_{k=1}^{N_d} a_k (i\omega)^k} \tag{5}$$

For a proper fit to N modes, such as in eq. (2), $N_d = 2N$ and $N_n = 2N - 1$. The numerator order can be increased with the denominator order held constant to account for out of band effects. This is done by setting

$N_n = 2N - 1 + N_{ex}$ where N_{ex} is the number of extra terms desired. The polynomials $(i\omega)^k$ will be written as functions of frequency $\Omega_k(\omega) = (i\omega)^k$, as done in [16] and [17]. Doing so allows the algorithm presented here to also be applied to a discrete-time model like those of the LSCF or LMS Polymax algorithms, where $\Omega_k(\omega) = \exp(-i\omega k T_s)$ with T_s being the sample time. Other possibilities for $\Omega_k(\omega)$ are Forsythe orthogonal polynomials, as used in the Rational Fraction Polynomial (RFP) algorithm [40] and [25], or Chebychev polynomials [28]. For generality, a scalar, frequency dependent weighting function $W(\omega)$ is introduced. This could be used, for example, to implement Sanathanan and Koerner's iterative method [29] [30]. In matrix form, the result of clearing the denominator of eq. (5) at a specific frequency can be expressed as

$$\left[W(\omega) \{H_p(\omega)\} [\Omega_0(\omega) \cdots \Omega_{N_d}(\omega)] \vdots - W(\omega) [\Omega_0(\omega) [I_{N_o}] \cdots \Omega_{N_n}(\omega) [I_{N_o}]] \right] \{\alpha\beta\} = \{0\} \tag{6}$$

where

$$\begin{aligned} \{\alpha\beta\} &= \left[a_0\, a_1 \cdots a_{N_d} \{B_0\}^T \{B_1\}^T \cdots \{B_{N_n}\}^T \right]^T \\ &= \left[\{\alpha\}^T \{\beta\}^T \right]^T \end{aligned} \tag{7}$$

and $[I_{No}]$ is an $N_o \times N_o$ identity matrix. An overdetermined set of equations can be formed by recognizing that $\{\alpha\beta\}$ are common factors at all frequencies, and then stacking block rows of eq. (6). Each block row has N_o rows. If data for N_f frequencies is included an overdetermined linear system $[J]\{\alpha\beta\} = \{0\}$ results, where the Jacobian matrix $[J]$ has dimensions $(N_o N_f) \times (N_d + N_o N_n)$. The name 'Jacobian' for the matrix $[J]$ comes from the derivation of the linear least squares algorithm [31].

Because the Jacobian matrix is complex, the equations $[J]\{\alpha\beta\} = \{0\}$ are complex even though $\{\alpha\beta\}$ is real. A real system of equations is needed to force $\{\alpha\beta\}$ to be real. This can be obtained by separating each equation into real and imaginary parts and requiring that both be satisfied. Forming the normal equations for the linear least squares problem as $\mathrm{Re}\left\{ [J]^H [J] \right\} \{\alpha\beta\} = \{0\}$ yields the same result, where $(.)^H$ denotes the Hermitian. Because the Jacobian matrix $[J]$ can be quite large and quite sparse if many frequencies and/or outputs are included, a much more efficient algorithm results if the normal equations $\mathrm{Re}\left\{ [J]^H [J] \right\} \{\alpha\beta\} = \{0\}$ are formed directly, rather than forming $[J]$ and evaluating $\mathrm{Re}\left\{ [J]^H [J] \right\}$. The normal equations are

$$\mathrm{Re}\left\{ [J]^H [J] \right\} \{\alpha\beta\} = \begin{bmatrix} [A_{11}] & [A_{12}] \\ [A_{12}]^H & [A_{22}] \end{bmatrix} \{\alpha\beta\} = 0 \tag{8}$$

where

$$[A_{11}] = \mathrm{Re}\left(\sum_{j=1}^{N_f}|W|^2\left(\{H_P\}^H\{H_P\}\right)\left\{\begin{array}{c}\Omega_0^*\\ \vdots\\ \Omega_{Nd}^*\end{array}\right\}\left[\begin{array}{ccc}\Omega_0 & \cdots & \Omega_{Nd}\end{array}\right]\right) \tag{9}$$

$$[A_{12}] = -\mathrm{Re}\left(\sum_{j=1}^{N_f}|W|^2\left\{\begin{array}{c}\Omega_0^*\\ \vdots\\ \Omega_{Nd}^*\end{array}\right\}\left[\begin{array}{ccc}\{H_P\}^H\Omega_0 & \cdots & \{H_P\}^H\Omega_{Nn}\end{array}\right]\right) \tag{10}$$

$$[A_{22}] = \mathrm{Re}\left(\sum_{j=1}^{N_f}|W|^2\left\{\begin{array}{c}\Omega_0^*[I_{N_o}]\\ \vdots\\ \Omega_{Nn}^*[I_{N_o}]\end{array}\right\}\left[\begin{array}{ccc}[I_{N_o}]\Omega_0 & \cdots & [I_{N_o}]\Omega_{Nn}\end{array}\right]\right) \tag{11}$$

or equivalently,

$$[A_{22}] = \mathrm{Re}\left(\sum_{j=1}^{N_f}|W|^2\left(\left\{\begin{array}{c}\Omega_0^*\\ \vdots\\ \Omega_{Nn}^*\end{array}\right\}\left[\begin{array}{ccc}\Omega_0 & \cdots & \Omega_{Nn}\end{array}\right]\right)\otimes[I_{N_o}]\right) \tag{12}$$

In the preceding $\otimes$ denotes the Kronecker product, defined as follows, where C_{ij} is the ijth element of $[C]$,

$$[C]\otimes[D] = \left[\begin{array}{ccc}C_{11}D & C_{12}D & \cdots\\ C_{21}D & C_{22}D & \cdots\\ \vdots & \vdots & \ddots\end{array}\right]$$

Note that in the first block row of eq. (8) the partition $[A_{11}]$ multiplies the denominator coefficients $\{\alpha\}$, while the partition $[A_{12}]$ multiplies the numerator coefficients $\{\beta\}$. Further computational savings result from a two-step solution procedure in which the denominator coefficients are found first. This is done by using the lower partition of eq. (8) to solve for $\{\beta\}$

$$\{\beta\} = -[A_{22}]^{-1}[A_{12}]^H\{\alpha\} \tag{13}$$

which is simplified by the identity $([C]\otimes[D])^{-1} = [C]^{-1}\otimes[D]^{-1}$ [32]. Use of this identity requires computation of the inverse of a relatively small N_n square matrix, rather than a much larger N_oN_n matrix. Substitution of eq. (13) into the upper partition of eq. (8) results in

$$\left[[A_{11}] - [A_{12}][A_{22}]^{-1}[A_{12}]^H\right]\{\alpha\} = [M]\{\alpha\} = \{0\}. \tag{14}$$

An additional constraint must be imposed in order to find a solution for the coefficients $\{\alpha\}$. One common approach, the least squares solution (LS), is to constrain the highest coefficient $a_{N_d} = 1$. Another alternative, the so called mixed least squares - total least squares solution (LS-TLS) is presented in [17] as $\{\alpha\} = \{v_{\min}\}$ where $\{v_{\min}\}$ is the eigenvector corresponding to the minimum eigenvalue of $[M]$. The authors have found a slight reduction in bias in some cases when using this mixed LS-TLS solution. For the problems presented in this paper, the LS-TLS algorithm is used. Also, only a single mode is fit ($N = 1$) so that $N_d = 2$ and $N_n = 1 + N_{ex}$ with $N_{ex} = 1$ or 2 typically.

3 Test Problem: Cantilevered Frame

No single test problem can capture every difficulty that could occur in a real experiment. The intent of the first problem is to capture the effect of varying noise levels, weakly excited and localized modes, and close modes. It has been used to assess previous implementations of AMI [11], [18], [19]. The problem was described in detail in [11], where the SISO version of AMI was used with the identical data set. The system consists of two orthogonal cantilevered beams, welded at their free ends, as depicted in Figure 1. *[Figure 1 frame layout 4.wmf about here]* The flexure and torsion effects were modeled using a constrained version of the Ritz method as described in Ginsberg [23]. The twenty-one lowest eigenvalues and associated mode functions obtained from a Ritz series analysis of the system were used to construct the impulse response resulting from excitation at one meter from the clamped support of the first beam. ($P = 1$, in eqs (2) and (15).) The identification that follows was focused on a band of frequencies containing only the lowest 11 modes, mimicing a real experiment in which many modes can exist beyond the frequency band of the analysis. The eigenvalues for these modes are shown in Table 1. *[Table 1 about here]*

The displacement and rotation as a function of time at seven points on the structure due to the impulsive force were synthesized from the Ritz series. The resulting response vector $\{y(t)\}$ contains both displacements and rotations at locations one meter apart,

$$\{y(t)\} = [w_1\ w_2\ w_3\ w_4\ \theta_1\ \theta_2\ \theta_3\ \theta_4\ w_5\ w_6\ w_7\ \theta_5\ \theta_6\ \theta_7\ \theta_8]^{\mathrm{T}} \tag{15}$$

where the first eight elements are measured on the first beam and the last seven elements are measured on the second beam.

The analytical responses were sampled, taking care to satisfy the Nyquist criterion, and then contaminated with noise by adding Gaussian white noise scaled to have a standard deviation of 1% of the maximum of each impulse

response. As a result, the dominant modes were not affected significantly by the noise, while the weakly excited modes were dominated by noise in some measurements. The AMI and the Stochastic Subspace Identification (SSI) [5] algorithms were both applied to the noise contaminated data set, and the resulting natural frequencies and damping ratios were compared. A Monte Carlo simulation was performed in order to verify that the results obtained were independent of the noise profile used. Towards this end, thirty different noise profiles were used, and the modal parameters obtained from each noise profile were stored for comparison. This approach allows one to characterize the scatter and bias in the modal parameters obtained by each algorithm. In the following, each algorithm will first be applied to a representative data set, following which the results of the Monte Carlo simulation will be presented.

The Stochastic Subspace Identification algorithm [5] was used to process the noise contaminated analytical data for the L-shaped frame, in order to provide a benchmark for the AMI algorithm. The specific stochastic algorithm used was included in the software tools supplied with [5] implemented in the function "subid.m." For more detail, see [3] or [5]. SSI begins by arranging the data into a large Hankel matrix. The R-factor in a QR decomposition of this Hankel matrix is found, following which a singular value decomposition of the R-factor is computed. The Hankel matrix has $2N_{br} * N_o$ rows, where the number of block rows in the Hankel matrix N_{br} is a user specified parameter, but the number of columns must exceed the number of rows. The algorithm used in this work required the Hankel matrix to be formed in memory. Because this problem used relatively few responses ($N_o = 15$), good results could be obtained using the limited memory available. The algorithm documentation suggested a formula for determining the number of block rows to use: $N_{br} = 2 * (maxorder) \,/\, (\#outputs)$ where $maxorder$ is the maximum model order to be estimated and $\#outputs$ is the number of outputs. For 11 modes (model order of 22) and 15 outputs as in this problem, $N_{br} = 4$. Trial and error indicated that the algorithm performed poorly unless many more block rows ($N_{br} \geq 32$) were used. Because the memory available in Matlab was limited, it was necessary to reduce the length of the time record in order to increase the number of block rows. The eigenvalues returned by SSI improved significantly as the number of block rows was increased, while they did not seem to be affected significantly by the length of the time record. In the results presented here, the first 8192 points of the time domain impulse response were processed, corresponding to the first 1.775 seconds of the response.

In [24] the effect of the number of block rows used in SSI was explored. The variation of the eigenvalues as a function of model order for a fixed number of block rows was also presented. It was found that for $N_{br} \geq 16$ very

clear stabilization diagrams were obtained, though many more block-rows were needed to obtain accurate results, especially for the damping ratios. The close modes 8 and 9 were distinctly identified only for $N_{br} \geq 32$. Furthermore, a bias error essentially constant with model order was identified, so that a convergent stabilization diagram was not necessarily an indication of accurate results. The results in [24] suggest that the best practice might be to create a stabilization diagram for increasing N_{br}, though this would be computationally demanding. In what follows, only the results for $N_{br} = 64$ will be presented, which were the best results obtainable by the algorithm with the limited memory available. A stabilization diagram for $N_{br} = 64$ is shown in Figure 2. *[Figure 2 'SSI_SD_i64.eps' about here.]* The composite FRF is overlaid for reference. Note that the model order on the right vertical axis is the number of underdamped modes in the SSI fit, or 1/2 the size of the state space $[A]$ matrix (see [5]). As shown in [24], the spurious poles are easily identified as they have higher damping ratios than the true poles.

SSI identified all modes in the frequency range of interest, including the highly localized, weakly excited mode 8, but doing so required that the model order exceed 20. Recall that 21 modes were used to construct the analytical impulse response, and that the time domain data processed by SSI was not filtered to limit the effect of modes outside of the band of interest. In some studies in the literature, the data analyzed in SSI are low pass filtered prior to processing in order to limit the influence of out of band modes, yet applying a filter to the data also increases the apparent model order seen by SSI [38]. For this problem, only ten modes exist beyond the maximum frequency of interest, and a relatively high order filter might be needed to adequately supress their contributions. Also, the results could vary depending on parameters chosen for the low-pass filter, and there does not appear to be a standard choice. For these reasons, the time responses were not filtered prior to applying SSI.

The errors in the natural frequency and damping ratio for each mode for each of the thirty different random noise profiles will be presented subsequently. In each trial, the eigenvalues for a model order of 21 will be used. In [24] the authors observed that the errors in the eigenvalues were not a strong function of the model order used, and that any model order greater than 20 seemed to give similar results.

In order to apply AMI to the noise contaminated impulse responses, it was first necessary to perform an FFT to convert them to frequency response functions. In doing so, the usual practice is to use a time window long enough to allow the impulse response to decay to a small fraction of it's maximum amplitude by the end of the time record, in order to avoid leakage error in the FRFs. For the frame system, this required that the length of the impulse

responses exceed 14.2 seconds or 65,536 samples. A relatively long time record is required by the slowly decaying, low frequency modes. However, the high frequency modes (8-11) have much larger real parts (see Table 1,) and thus decay quickly. The consequence is that use of a time record long enough to allow the low frequency modes to decay amplifies the effect of noise in the FFT for the high frequency modes, because at later times their contributions are below the noise. In such a situation an exponential window is often applied to the impulse responses to reduce the effect of noise. In order to eliminate any dependence on the exponential window factor and simplify the presentation, this approach was not used. Instead, AMI was applied to FRFs created from the first 8192 samples of the impulse response. While this resulted in leakage error in the FRFs, it allowed for AMI and SSI's results to be compared for the same data set represented in time and frequency domains. Furthermore, leakage tends to contaminate the estimate of the mode vector scaling primarily, so that one might still obtain accurate estimates of the natural frequency, damping ratio, and mode shape even when leakage errors are present [1]. In [24] AMI was applied to FRFs obtained from an FFT applied to 65,536 samples of the noisy impulse response, yielding natural frequencies, damping ratios, and mode shapes that are similar to those presented here.

Figures 3 and 4 show typical noise contaminated rotation and displacement FRFs for the 8192 sample time records. Eleven modes are present in the frequency band of interest, but the high frequency modes (8-11) were barely visible in the noise-contaminated displacement data, as typified by Figure 4. In contrast, the higher frequency modes are fairly well represented in the rotation data, as seen in Figure 3. Only a single peak is evident in the vicinity of modes 8 and 9. *[Figures 3 and 4 'Frame_ex_FRFs.eps' about here]*

AMI begins with the subtraction phase, in which modes are sucessively identified and subtracted from the data set. After each subtraction step, composite FRFs were formed to assess the quality with which the identified mode matched the data. Toward this end, all identified modal properties are utilized to synthesize individual FRFs in eq. (2). Composites of both the residual FRFs and the synthesized FRFs were then constructed according to eq. (3) and compared. Nyquist plots can also be helpful in assessing the quality of fit, though simultaneously considering the Nyquist plots of a large number of FRFs can be tedious, and there does not seem to be a standard definition of a composite FRF that retains phase information. The composites formed by eq. (3) can not be used to create a Nyquist plot because they contain no phase information. Simple addition of FRFs can lead to cancellation of some modes' contributions, depending on their spatial phase. For example, adding FRFs for a symmetric structure would

tend to reinforce symmetric modes while annihilating antisymmetric modes. For this reason a Nyquist composite FRF is defined herein as a weighted sum of the FRFs using the elements of the residue vector $\{(A_{\text{fit}})_r\}$ as weights. Use of the residue vector for mode r tends to reinforce mode r in the sum. Specifically, the condensed FRF data $(H_{\text{cn}})_r(\omega)$ is defined mathematically as

$$(H_{\text{cn}})_r(\omega) = \{(A_{\text{fit}})_r\}^H * \{H_{\text{res}}(\omega)\} \tag{16}$$

where $\{(A_{\text{fit}})_r\}$ is the current estimate of the residue matrix for the mode whose quality of fit is being assessed and $\{H_{\text{res}}(\omega)\}$ is residual FRF data to be condensed. The data $(H_{\text{cn}})_r(\omega)$ can be plotted in the complex plane, resulting in what shall hereafter be referred to as a 'Nyquist composite plot.'

The procedure for each subtraction step is summarized as follows. The algorithm begins by fitting a mode to the data surrounding the peak in the composite FRF, $H_{\text{c}}(\omega)$ in eq. (3), formed from the residual FRF data. The parameters for the identified mode are used to synthesize the FRFs. The synthesized FRFs are compared with the residual FRFs by comparing a composite FRF, $H_{\text{c}}(\omega)$ in eq. (3), and a Nyquist composite FRF, $(H_{\text{cn}})_r(\omega)$ in eq. (16), of each. If the agreement is deemed acceptable, the modes are accepted and subtracted from the residual FRF data and a new subtraction step begins. If unacceptable agreement is obtained, the algorithm either proceeds to a different frequency interval or the subtraction phase ceases. This is illustrated for the last few subtraction steps on the frame data in Figure 5. Each row of panes displays the data at a single subtraction step. The pane on the left shows a composite FRF formed from the residual FRFs at the current subtraction step and a composite FRF formed from the synthesized or 'fit' FRFs for the mode identified in the current subtraction step. The pane on the right shows Nyquist composite FRFs of the same, both of which are created using the residue for the mode identified in the current subtraction step in eq. (16).

[Figure 5 'AMI_sub_sr.eps' about here] After the tenth subtraction step a number of peaks are still evident in the data. Each of the peaks below 2000 rad/s is the result of small errors in fitting previously identified modes. Experience has shown that it is advisable to disregard these fitting errors during the subtraction phase, as they will usually disappear after mode isolation and refinement. One way of doing this is to zero the FRF data near each mode's resonant peak immediately after it is identified and subtracted from the data [11]. This was not done here, although attempts at fitting any of the peaks below 2000 rad/s resulted either in unstable modes or modes that when subtracted from the data set did not reduce the magnitude of the FRF data within the fit band. For these reasons,

all of the data below 2000 rad/s was neglected during the 11th subtraction step, bringing the peak near 2500 rad/s into dominance. This peak is outside of mode nine's half-power bandwidth (Step 9 in Figure 5,) suggesting that is it indeed due to a distinct mode. The data near 2500 rad/s is fit with only fair accuracy, though the Composite Nyquist plot (or alternatively a standard Nyquist plot for a well chosen response point) shows a definite arc, indicative of a true mode, so it was retained. After this mode is subtracted the data appears totally incoherent, so subtraction ceased with eleven modes identified. After the subtraction phase, AMI proceeds to mode isolation. Twenty-nine iterations were performed on this data, at which juncture the maximum change in either eigenvalues or residues was 0.001%.

In [11] the authors applied the SISO AMI algorithm to a similar data set, noting that not all of the modes were identifiable in each FRF. As a result, it was not always easy to tell when one should halt the subtraction phase, and user interaction was required for each FRF. In contrast, with the global algorithm there was no ambiguity concerning when to stop looking for modes, as illustrated by Figure 5. After step eleven there was clearly no indication of a mode with a global effect. As a result, user interaction and processing time were greatly reduced for the global algorithm.

[Figure 'Frame_MCres.eps' about here]

When AMI was applied to some of the noise contaminated data sets comprising the Monte Carlo simulation with $\alpha = 0.707$, (see eq. (4)), the data selected for fitting mode 9 fell in a frequency band that overlapped the band for mode 8. This led to a divergent situation when the algorithm proceeded to mode isolation. The divergence was recognizable by modes eight and nine converging towards nearly equal eigenvalues, with equal and opposite residue vectors that steadily increased in magnitude. Experimentation revealed that using $\alpha = 0.75$ reduced the frequency interval for each fit sufficiently to avoid this problem. This allowed the Monte Carlo simulations to be performed automatically by AMI.

The percent errors in the natural frequencies and damping ratios obtained in each of 30 trials are plotted in Figure 6. The distribution of these errors illustrates the bias and scatter of the algorithms. The scatter is characterized by the width of the distributions, higher scatter indicating that larger errors are possible for any given noise profile. The center of the distributions defines the bias. A bias different from zero represents the average error obtained when the experiment is repeated a number of times. For modes 8-11 the algorithms gave comparable results, though

AMI shows a large bias error in the damping ratio for mode 8. AMI's estimates of the natural frequencies and damping ratios of modes 1-7 show much less scatter than SSI's. The bias errors for modes 1-7 of the two algorithms are comparable, even though the FRFs processed by AMI showed considerable leakage error in the peaks of these modes. On average, the standard deviations of SSI's estimates for the damping ratios of modes 1-7 were 6.7 times higher than the standard deviations of AMI's estimates.

As reported in [24], when using the SSI algorithm, a very clear stabilization diagram is also obtained with 32 block rows in the data Hankel matrix. A Monte Carlo simulation using 32 block-rows in the SSI algorithm was also performed. The standard deviations of the natural frequencies and damping ratios of modes 1, 2, and 8 for the 32 block-row case were more than twice those for the 64 block row case, while the parameters of most of the other modes had similar means and standard deviations for 32 and 64 block rows.

4 Z24 Bridge Data

4.1 Data Description & Signal Processing

In order to demonstrate the performance of the AMI algorithm on experimental data, an analysis of drop-test data from the Z24 bridge in Switzerland is presented. This data was made publicly available by researchers at the Katholieke Universiteit Leuven and is available at: *http://www.kuleuven.ac.be/bwm/IMAC/*. A number of researchers analyzed the data and presented their results at the 19th International Modal Analysis Conference, see [8], [33], [34], [35], [36] and [37]. A more detailed description of the system and data acquisition is available in these articles.

The Z24 bridge was excited by dropping a large mass (approximately 100 kg) onto the bridge a number of times and recording the response with accelerometers. Because of the size of the bridge, the response was measured in nine setups of up to 15 sensors each, with three sensors common to all setups. There were a total of 99 response measurements at 75 different locations. In most of the setups the mass was dropped four times. Because the excitation approximates an impulse, the (unscaled) FRFs are approximated by the FFT of the response. The time series were broken into segments representing individual impulse responses by triggering the signal from node 2 in the vertical direction (one of the reference sensors), resulting in a set of (usually) four impulse responses per time

record. The individual impulse responses for each sensor were then truncated or zero padded to a length of 1024 samples. The FFTs for each 1024 length response found with a rectangular window were then averaged. This was performed for each setup resulting in a total of 99 frequency responses processed globally by AMI.

Globally processing all of the frequency responses allowed for all available information to be used when estimating the modal parameters. Because three sensors were common to each of nine setups, nine repetitions of the measurements for these sensors were available. These were retained as if they had been distinct measurement channels, so that the mode shapes could be 'glued' together in the following manner. If the frequency responses due to the drop excitation are assumed to be flat within the bandwidth of each mode, then the residues obtained for each mode would be proportional to the true residues, the unknown scaling being a function of the magnitude and phase of the impulse excitation. Because the triggering was not perfect, this scaling was different for different measurement setups, (though consistent for all responses of a given setup.) This was evidenced by the fact that if the FRFs for the non-reference sensors were processed globally, the resulting mode shapes had visibly inconsistent magnitude and phase from patch to patch. With the reference sensors retained as individual measurement channels, the residues found at the reference sensors in each setup could be used to find a scale factor for all residues of the same setup, resulting in consistently scaled mode shapes.

4.2 Analysis with AMI-SIMO

Initial tests on the Z24 data using the same peak selection factor α used for the frame data led to two difficulties. First, visual inspection of the peak data selected by the algorithm showed that often more than one peak was included in the frequency band, causing the SDOF fitting algorithm to give erroneous results. Second, a pair of modes was identified whose fitting bands overlapped significantly, resulting in divergence of their modal parameters in the mode isolation phase. These problems could have been corrected by manually adjusting the fitting bands. However, use of a peak selection factor of 0.8 allowed for semi-automatic processing of the data. Furthermore, use of more data around the peaks did not appear to give better results for any of the modes. One extra numerator term was used in all fits to account for out of band effects. Figures 7 and 8 describe the composite FRF and fit for eight subtraction steps. A composite Nyquist plot is shown to the right for each subtraction step.

When subtraction step eight is reached, data at the high frequency end of the frequency band becomes dominant. Visual inspection of this data suggests that it is due to out of band modes. For this reason, the high frequency data

was nullified in the residual for subtraction step eight (shown lighter in Figure 8,) causing the peak near 12 Hz to come into dominance. After step eight, peaks due to fit errors in previously identified modes become dominant in the data. Attempting a fit in any of these regions results either in a nonphysical mode ($\zeta < 0$) or a mode with an eigenvalue that is very similar to that of a previously identified mode. For this reason, subtraction was halted with eight modes identified. After mode isolation and refinement the residual, formed by subtracting the contributions of all identified modes, was searched again for evidence of any additional modes, but none were found.

The algorithm next proceeds to mode isolation, converging after 29 iterations. The synthesized composite FRF after mode isolation and refinement, shown in Figure 9, agrees quite well with the composite FRF of the data. The difference between the fit and data is 1-2 orders of magnitude. Individual reconstructed FRFs also agreed well with the FRF data.

Figures 7 and 8 show that during subtraction, the agreement between the residual FRFs and the synthesized FRFs is only fair for some of the identified modes. However, the composite Nyquist plot in each case did show a circular arc indicative of a true mode, so the modes were retained. After mode isolation, composites of the synthesized FRFs for individual modes were compared to composites of the isolation residual FRFs. (The isolation residual is the data fit in the mode isolation phase, defined in [22] as the original FRF data minus the contributions of all identified modes except for the mode in focus.) The agreement between the Nyquist composite of the isolation residual for each individual mode and the Nyquist composite of the synthesized FRF was excellent for all of the modes except for modes 4 and 5. Consequently, one would expect the modal parameters for modes 4 and 5 to be less accurate than those of the other modes. Investigation revealed that the algorithm was selecting data well outside of the half power bandwith for the fit to modes 4 and 5. Further experimentation revealed that the quality of fit for modes 4 and 5 increased greatly if a peak selection factor of $\alpha = 0.9$ and zero extra numerator terms were used for these modes, while using $\alpha = 0.8$ and one extra numerator term for all of the other modes.

[Tables 2 and 3 about here] The natural frequencies and damping ratios found by AMI using $\alpha = 0.8$ and one extra numerator term for all modes are presented in Tables 2 and 3. These results represent the best results the authors could obtain using the SIMO-AMI algorithm operating in a semi-automatic fashion. The results found for modes 4 and 5 when using $\alpha = 0.9$ and zero extra numerator terms are also shown, marked with an asterix (*). These latter results are preferred as they resulted in a greatly improved fit for modes 4 and 5.

The natural frequencies and damping ratios reported by Marchesiello *et al* [8], Luscher *et al* [33], Schwarz and Richardson [34], [35]and Fasana *et al* [37] are also presented in Tables 2 and 3. Some of the aforementioned researchers presented the results of analyzing other data sets taken from the bridge, though only the results for the drop tests data are shown here. Marchesiello *et al* [8] processed the bridge data using an SSI algorithm very similar to that used in the previous section. They processed the data globally setup by setup, so that no more than 15 responses were processed simultaneously. Fasana *et al* analyzed the data using the Ibrahim Time Domain algorithm and the Auto Regressive Moving Average Vector ARMAV algorithm, reporting that the ARMAV algorithm gave better results. Fasana *et al* processed the data setup by setup, and in each setup they split the frequency band into 2-4 segments to limit the number of modes in each analysis band. Luscher *et al* used the Frequency Domain Decomposition (FDD) algorithm and the Eigensystem Realization Algorithm (ERA) to process the drop test data, reporting that better results were obtained by the FDD algorithm. The results presented in Tables 2 and 3 for Luscher are the result of the FDD algorithm applied globally to the data from all setups, denoted the 'FDD2' results in [33]. Schwarz and Richardson applied a rational fraction polynomial curve fit to 'ODS FRFs' created from the response data to find the natural frequencies, damping ratios and mode shapes from the drop-test data. The auto and cross spectra between each output sensor and the reference sensors were combined to form three sets of ODS FRFs, one for each reference, and each set was curve fit independently. The natural frequencies and damping ratios in Tables 2 and 3 are the averages of those found from the three sets of ODS FRFs. The standard deviation is shown in parenthesis for all modes identified in at least two sets of ODS FRFs.

The values found by AMI agree well with those published by other researchers. Modes 4 and 5 were missed by Luscher *et al* and Schwarz and Richardson. Fasana *et al* also missed modes 4 and 5 when using the ITD algorithm, (the results of the ITD algorithm are not reproduced in Tables 2 and 3.) The ARMAV algorithm enabled them to identify all of the modes in Tables 2 and 3 except for mode 4. Marchesiello *et al* found a mode at 19.78 Hz, having a mode shape similar to that for mode 8, which was not identified by any of the other researchers. Both Marchesiello *et al* and Schwarz and Richardson found modes near 26 Hz, which were just outside the frequency band analyzed by AMI. Visual comparison of the mode shapes found by AMI with those presented by other researchers found them to be in good agreement.

Wire-frame plots of SIMO-AMI's mode shapes are shown in Figures 10 through 17. In order to plot the mode

shapes, the real displacement response in each mode was found at the instant when it is an overall maximum. This was accomplished by multiplying each mode shape $\{\psi\}$ by $e^{i\theta}$, with θ found to maximize the realness of the the product $\{\psi\}\, e^{i\theta}$, and then plotting the real part of $\{\psi\}\, e^{i\theta}$, (solid lines in Figures 10 through 17). The imaginary part of $\{\psi\}\, e^{i\theta}$ is also shown in Figures 10 through 17 by a dash-dot line. Inspection of Figures 10 through 17 reveals that the imaginary parts are generally much smaller, indicating that most of the modes had good modal phase collinearity [1]. However, one can see that the imaginary parts are quite significant for modes 4, 5 and 7. Considering that these modes are not very heavily damped, the complexity of their mode vectors is likely due to signal processing errors (i.e. leakage, etc...), or errors in the identification. Visual comparison of the mode shapes in Figures 10 through 17 with those presented by other researchers found them to be in good agreement, with the exception of modes 5 and 7 for which the agreement was fair.

5 Conclusion

A simple, computationally efficient, global single–input-multi-output MDOF fitting algorithm has been presented and implemented in SDOF form as a part of the Algorithm of Mode Isolation (AMI). One benefit of the global algorithm is a great reduction in user interaction when compared to the SISO AMI algorithm, and greater ease in determining the number of modes contributing to the response. On the other hand, usage of a global algorithm might cause highly localized modes to go undetected, as noted in [24]. A SISO algorithm, which examines each FRF, is less likely to miss the occurrence of localized modes if one has adequately sampled the structure spatially. However, when using a SISO algorithm, it may be difficult to determine the number of distinct eigenvalues in each frequency band, as discussed in [11].

The stochastic subspace identification algorithm of Van Overschee and De Moor was also applied to the frame data. SSI was found to give good results, so long as a sufficient number of block rows were used in the data Hankel matrix. The computation time for the SSI algorithm was much longer than for AMI. Because of memory limitations, SSI only processed the first 8192 samples of the impulse response. In order to assure that neither AMI nor SSI benefited nor was penalized by using more or less of the data, AMI was applied to FRFs derived from only the first 8192 samples of the elastic frame's impulse response. Monte Carlo simulations revealed that AMI more accurately identified the eigenvalues of the lightly damped modes of the structure, while AMI and SSI gave comparable accuracy for modes 9-11, whose damping is substantially greater than the first seven modes. On the other hand, AMI showed

considerable bias in identifying the damping ratio of the 8th mode. Considering the high noise level in the vicinity of mode eight, this could be a case in which the systematic contribution of noise to a linear least squares fit causes a bias. Finally, it should be noted that while every effort was made to provide a fair comparison between AMI and SSI, several special operations were mentioned that could have been applied to benefit either AMI or SSI, illustrating some of the practical issues involved in selecting between time and frequency domain identification. These operations might be carried out by an experienced operator, based on considerations that were discussed.

As noted previously, when SSI was applied with 16 block rows in the data Hankel matrix, a single mode was visible on the stabilization diagram in the frequency range of modes eight and nine. Modes eight and nine were distinctly identified when 32 or 64 block rows were used, with the accuracy of the resulting modal parameters increasing significantly as the number of block rows in the Hankel matrix increased. A corollary of these observation is that for some problems, (especially those with many outputs) constraints on memory or processing time may result in the SSI algorithm missing modes or achieving sub-optimal estimates of the modal parameters. The situation is further complicated by the observation in [24] that very clear stabilization diagrams can be obtained even when the number of block rows is too small to result in accurate modal parameters. Indeed, for this problem there was little noticeable difference in the clarity of the stabilization diagrams for 16, 32 or 64 block rows.

The difficulty in identifying systems having modes with a wide range of decay constants was illustrated by the elastic frame problem. The effect of noise on the quickly decaying modes of the structure was more drastic when longer time records were used (see [24]), though use of a shorter record as done herein resulted in leakage errors for the slowly decaying modes. These leakage errors had a minor effect on the accuracy of the natural frequencies and mode shapes of these modes, and resulted in only moderately larger errors in the damping ratios, though considerable error in the modal scale factors was observed. Further experimentation (not presented here) revealed that applying an exponential window to the impulse response data reduced these scale errors, without decreasing the accuracy of the natural frequencies and damping ratios significantly.

The final section of this paper presented an analysis of drop test data for the Z24 Bridge, in order to demonstrate the application of AMI to real experimental data. Considerations for determining the number of modes active in the frequency band with AMI were discussed, and AMI's results were found to agree well with those presented by other researchers, some of whom did not identify all of the modes. It was demonstrated that AMI provides a

clear indication of the quality of the fit for each individual mode. Furthermore, the algorithm is flexible, so that an experienced user might manually intervene, based on guidelines discussed in the paper, if anomalous results are obtained. The computation time required to globally process all 99 FRFs of the Z24 bridge was relatively short. In general, AMI's short processing time is a result of fitting only data near the peaks, using simple, low order fitting techniques.

ACKNOWLEDGEMENT OF SUPPORT

This material is based on work supported under a National Science Foundation Graduate Research Fellowship.

References

[1] R. J. Allemang, *Vibrations Course Notes*, http://www.sdrl.uc.edu/, Cincinnati, 1999.

[2] R. J. Allemang and D. L. Brown, "A unified matrix polynomial approach to modal identification," *Journal of Sound and Vibration*, vol. 211, no. 3, (1998) pp. 301–322.

[3] K. De Cock, B. Peeters, A. Vecchio, B. De Moor, and H. Van Der Auweraer, "Subspace system identification for mechanical engineering," *Proceedings of ISMA2002 - International Conference on Noise and Vibration Engineering*, Leuven, Belgium, vol. III, 2002, pp. 1333–1352.

[4] S. W. Doebling, K. F. Alvin, and L. D. Peterson, "Limitations of state-space system identification algorithms for structures with high modal density," *12th International Modal Analysis Conference (IMAC-12)*, Honolulu, Hawaii, 1994, pp. 633–640.

[5] P. Van Overschee and B. De Moor, *Subspace Identification for Linear Systems: Theory-Implementation-Applications*, Kluwer Academic Publishers, Boston, 1996.

[6] I Goethals and B. De Moor, "Model reduction and energy analysis as a tool to detect spurious modes," *Proceedings of ISMA2002 - International Conference on Noise and Vibration Engineering*, Leuven, Belgium, vol. III, 2002, pp. 1307–1314.

[7] P. Verboven, E. Parloo, P. Guillaume, and M. Van Overmeire, "Autonomous modal parameter estimation based on a statistical frequency domain maximum likelihood approach," *19th International Modal Analysis Conference (IMAC-19)*, Kissimmee, Florida, 2001, pp. 1511–1517.

[8] S. Marchesiello, B.A.D. Piombo, and S. Sorrentino, "Application of the CVA-BR method to the 224 bridge vibration data," *19th International Modal Analysis Conference*, Kissimmee, Florida, 2001.

[9] H. Van Der Auweraer, W. Leurs, P. Mas, and L. Hermans, "Modal parameter estimation from inconsistent data sets," *18th International Modal Analysis Conference (IMAC-18)*, San Antonio, Texas, 2000, pp. 763–771.

[10] M. V. Drexel and J. H. Ginsberg, "Mode isolation: A new algorithm for modal parameter identification," *Journal of the Acoustical Society of America (JASA)*, vol. 110, (2001) 1371–1378.

[11] M. S. Allen and J. H. Ginsberg, "A linear least-squares version of the algorithm of mode isolation for identifying modal properties. part II: Application and assessment," *Journal of the Acoustical Society of America (JASA)*, vol. 116, (2004) 608–615.

[12] Kirshenboim, J., SIM - Modal identification by simultaneous mode fitting, Imperial College Dynamics Section Report No. 7914, London, Imperial College, 1979.

[13] D.A. Robb, User's Guide to Program MODENT, Department of Mechanical Engineering, Imperial College of Science and Technology, London, UK.

[14] H. P. Yin and D. Duhamel, "Subtraction technique and finite difference formulas for modal parameter estimation." *Mechanical Systems and Signal Processing*, vol. 18, (2004) 1497–1503.

[15] J. H. Ginsberg, M. S. Allen, A. Ferri, and C. Moloney, "A general linear least squares SDOF algorithm for identifying eigenvalues and residues," *21st International Modal Analysis Conference (IMAC-21)*, Orlando, Florida, 2003.

[16] P. Guillame, P. Verboven, S. Vanlaunduit, H. Van Der Auweraer, and B. Peeters, "A poly-reference implementation of the least-squares complex frequency-domain estimator," *International Modal Analysis Conference (IMAC XXI)*, Kissimmee, Florida, 2003.

[17] H. Van Der Auweraer, P. Guillame, P. Verboven, and S. Vanlaunduit, "Application of a fast-stabilizing frequency domain parameter estimation method," *Journal of Dynamic Systems, Measurement, and Control*, vol. 123, 2001, pp. 651–658.

[18] M. V. Drexel and J. H. Ginsberg, "Modal parameter identification using state space mode isolation," in *19th International Modal Analysis Conference (IMAC-19)*, Orlando, FL, 2001.

[19] M. V. Drexel, J. H. Ginsberg, and B. R. Zaki, "State space implementation of the algorithm of mode isolation," *Journal of Vibration and Acoustics*, vol. 125, (2003) 205–213.

[20] J. H. Ginsberg, B. R. Zaki, and M. V. Drexel, "Application of the mode isolation algorithm to the identification of a complex structure," *20th International Modal Analysis Conference (IMAC-20)*, Los Angeles, CA, 2002, pp. 794–801.

[21] J. H. Ginsberg and M. S. Allen, "Recent improvements of the algorithm of mode isolation," *Proceedings of IMECE'03, ASME International Mechanical Engineering Congress and Exposition, NCA*, Washington, DC, 2003.

[22] J. H. Ginsberg and M. S. Allen, "A linear least-squares version of the algorithm of mode isolation for identifying modal properties. part I: Conceptual development," *Journal of the Acoustical Society of America (JASA)*, vol. 116, 2004, pp. 600–607.

[23] J. H. Ginsberg, *Mechanical and Structural Vibrations*, John Wiley and Sons, New York, first edition, 2001.

[24] M. S. Allen and J. H. Ginsberg, "SIMO extension of the algorithm of mode isolation," *IMAC 22 - XXII International Modal Analysis Conference*, Dearborn, Michigan, 2004.

[25] D. Formenti and M. Richardson, "Parameter estimation from frequency response measurements using rational fraction polynomials (twenty years of progress)," *20th International Modal Analysis Conference (IMAC-20)*, Los Angeles, CA, 2002, pp. 373–382.

[26] P. Guillame, P. Verboven, S. Vanlaunduit, and E. Parloo, "Accurate damping estimates using adapted frequency-domain identification techniques," *International Modal Analysis Conference (IMAC XVIII)*, San Antonio, Texas, 2000, pp. 411–417.

[27] B. Cauberghe, P. Guillame, P. Verboven, and E. Parloo, "Identification of modal parameters including unmeasured forces and transient effects," *Journal of Sound and Vibration*, vol. 265, (2003) 609–625.

[28] P. Guillame, B. Peeters, B. Cauberghe, and P. Verboven, "Identification of highly damped systems and its application to vibro-acoustic modeling," *International Modal Analysis Conference (IMAC XXII)*, Dearborne, Michigan, 2004.

[29] C. K. Sanathanan and J. Koerner, "Transfer function synthesis as a ratio of two complex polynomials," *IEEE Transactions on Automatic Control*, vol. AC-9, no. 1, 1963, pp. 56–58.

[30] R. Pintelon, P. Guillame, Y. Rolain, J. Shoukens, and H. Van hamme, "Parametric identification of transfer functions in the frequency domain–a survey," *IEEE Transactions on Automatic Control*, vol. 39, no. 11, 1994, pp. 2245–2260.

[31] W. H. Press, S. A. Teukolsky, W. T. Vetterling and B. P. Flannery, *Numerical Recipes in Fortran*, Cambridge University Press, New York, second edition, 1992.

[32] J. W. Brewer, "Kronecker products and matrix calculus in system theory," *IEEE Transactions on Circuits and Systems*, vol. CAS-25, no. 9, 1978, pp. 772–781.

[33] D. J. Luscher, J. M. W. Brownjohn, H. Sohn, and C. R. Farrar, "Modal parameter extraction of 224 bridge data," *19th International Modal Analysis Conference*, Kissimmee, Florida, 2001.

[34] B. Schwarz and M. Richardson, "Post-processing ambient and forced response bridge data to obtain modal parameters," *19th International Modal Analysis Conference*, Kissimmee, Florida, 2001.

[35] B. Schwarz and M. Richardson, "Modal Parameter Estimation from Ambient Response Data," *19th International Modal Analysis Conference*, Kissimmee, Florida, 2001.

[36] K. Womack and J. Hodson, "System identification of the 224 swiss bridge," *19th International Modal Analysis Conference*, Kissimmee, Florida, 2001.

[37] A. Fasana, L. Garibaldi, E. Giorcelli, and D. Sabia, "Z24 Bridge Dynamic Data Analysis by Time Domain Methods," *19th International Modal Analysis Conference*, Kissimmee, Florida, 2001.

[38] B. Peeters and G. D. Roeck, "Reference based stochastic subspace identification for output-only modal analysis," Mechanical Systems and Signal Processing, vol. 13, no. 6, pp. 855—878, 1999.

[39] Levy, E.C., "Complex curve fitting," IRE Transactions on Automatic Control, vol. AC-4, pp. 37-44, 1959.

[40] Richardson, M. and D. Formenti. "Parameter Estimation from Frequency Response Measurements Using Rational Fraction Polynomials," *1st International Modal Analysis Conference (IMAC I)*, Orlando, Florida, 1982.

Mode	**Re{λ}**	**Im{λ}**	*Damp* $\zeta * 100$
1	-0.656461	68.0047	0.97
2	-0.164031	265.912	0.06
3	-0.482573	386.324	0.12
4	-0.267046	829.451	0.03
5	-0.793483	1033.75	0.08
6	-0.610694	1697.01	0.04
7	-3.1205	1937.89	0.16
8	-18.7961	2479.67	0.76
9	-18.1254	2510.98	0.72
10	-5.34622	2995.66	0.18
11	-5.21094	3380.04	0.15

Table 1: Eigenvalues for First 11 Modes

Natural Frequency (Hz), (σ Hz)					
Mode	AMI-SIMO	Marchesiello et al [8] SSI	Fasana [37] ARMAV	Luscher [33] FDD2	Schwarz & Richardson [35]
1	3.845	3.86 (0.01)	3.74	3.85	3.850 (0.002)
2	4.822	4.82 (0.01)	4.93	4.80	4.816 (0.027)
3	9.750	9.76 (0.05)	9.63	9.73	9.747 (0.006)
4	10.467 10.427*	10.43 (0.11)	-	-	-
5	11.616 12.188*	12.35 (0.12)	12.3	-	-
6	13.178	13.25 (0.09)	13.3	13.05	13.232 (0.196)
7	16.735	17.25 (0.31)	17.3	-	17.284
8	19.188	19.15 (0.08)	19.2	19.19	19.242 (0.019)

Table 2: Natural frequencies for Z24 bridge drop test data from various researchers. *Values found using a peak selection factor of 0.9 and zero extra numerator terms.

Damping Ratio (%), (σ %)					
Mode	**AMI-SIMO**	Marchesiello et al [8] SSI	Fasana [37] ARMAV	Luscher [33] FDD2	Schwarz & Richardson [35]
1	0.923	0.9 (0.14)	1.5	0.96	0.96 (0.00)
2	1.76	1.69 (0.25)	1.8	2.76	1.21 (0.08)
3	1.68	1.54 (0.31)	2.1	1.79	1.56 (0.04)
4	2.53 2.51*	2.53 (0.86)	-	-	-
5	8.45 3.68*	3.08 (1.02)	2.2	-	-
6	4.59	3.93 (0.37)	3.2	5.24	2.34 (0.88)
7	5.65	3.94 (0.56)	2.9	-	3.95
8	2.60	2.10 (0.53)	2.8	3.15	2.25 (0.12)

Table 3: Damping Ratios for Z24 bridge drop test data from various researchers. *Values found using a peak selection factor of 0.9 and zero extra numerator terms.

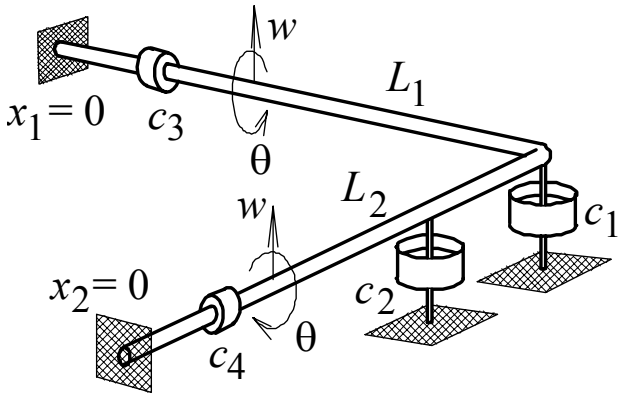

Figure 1: Cantilevered Frame System

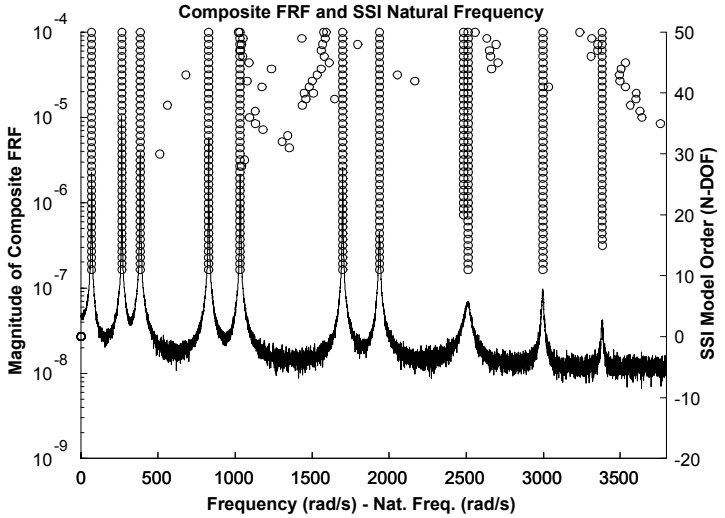

Figure 2: Stabilization diagram for SSI algorithm with 64 block rows and composite FRF for Frame data. SSI fit the time domain data directly; the compoiste FRF is shown only for reference.

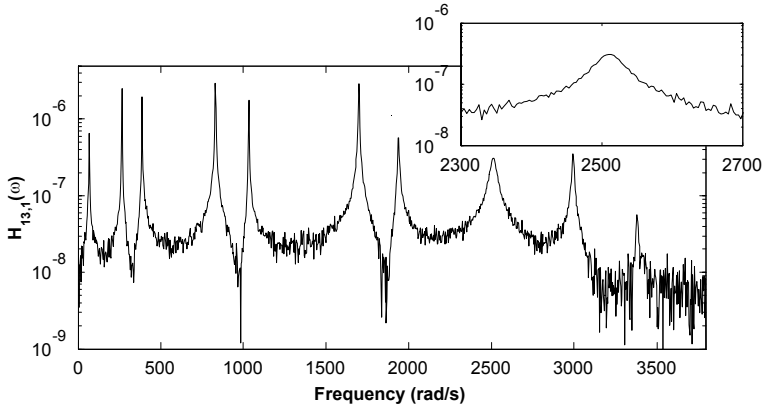

Figure 3: Noisy rotation FRF at 2 m from clamped support on beam 2.

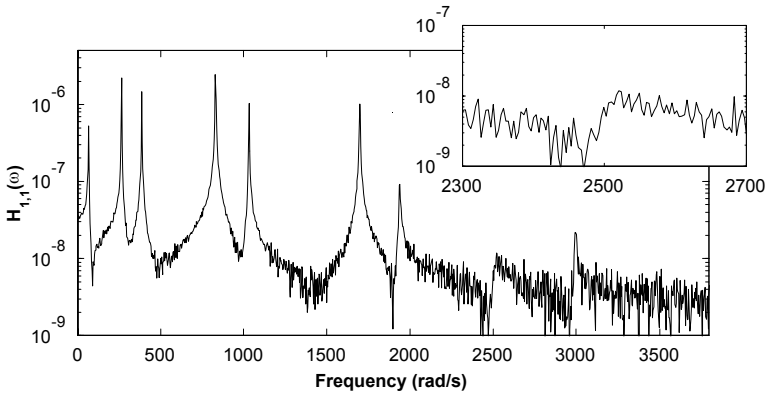

Figure 4: Noisy displacement FRF at 1 m from clamped support on beam 1.

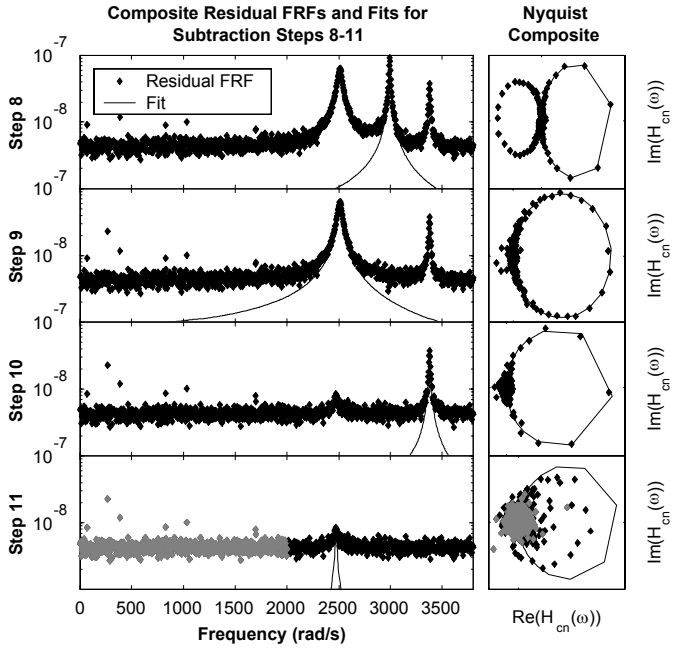

Figure 5: AMI Subtraction steps 8-11 for short record (8192 samples) frame data set. LEFT: Composite residual FRFs (.) and fits (-). RIGHT: Nyquist composite plots of residual FRF data (.) and fits (-). The data shown in gray in the bottom pane was ignored in Step 11.

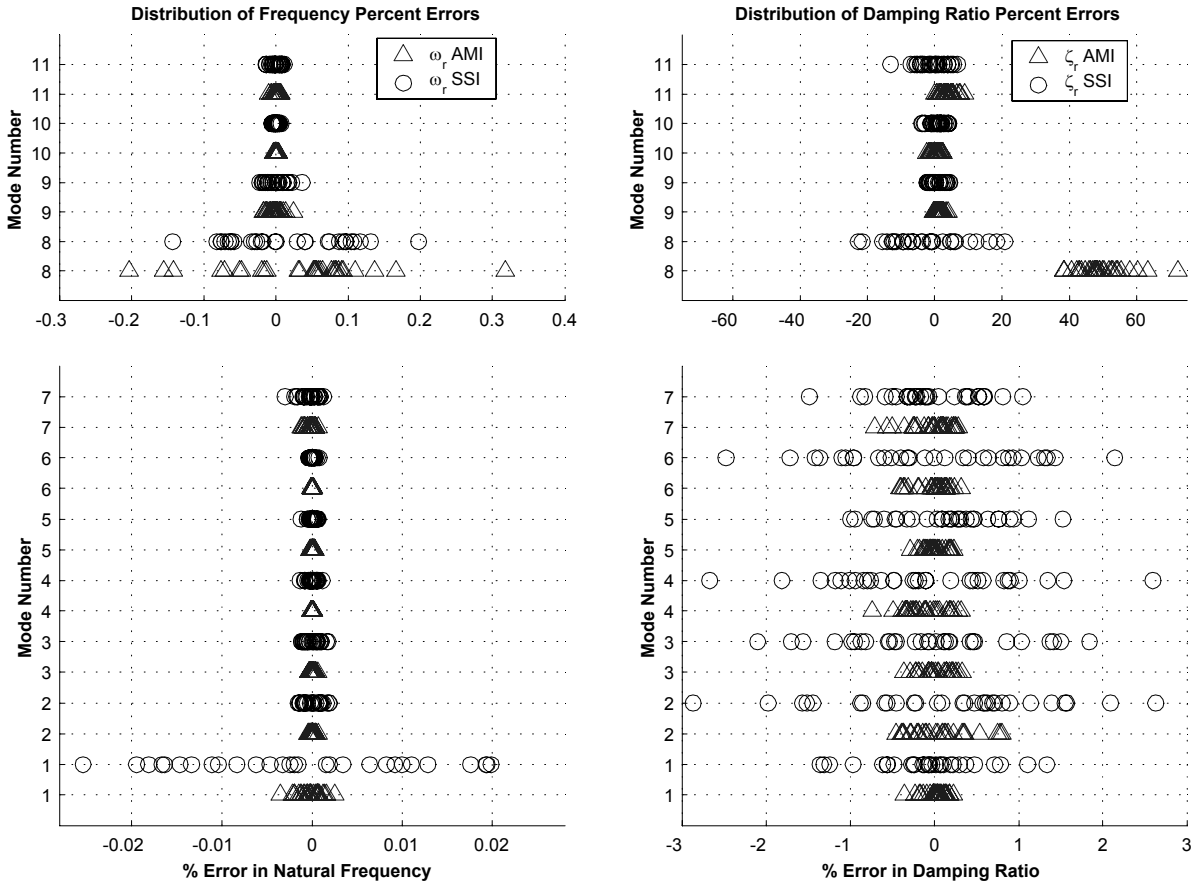

Figure 6: Monte Carlo Simulation Results for 8192 sample data from frame structure: Percent errors in Natural Frequency (left) and Damping Ratio (right) for AMI (triangles) and SSI (circles) for each of thirty trials.

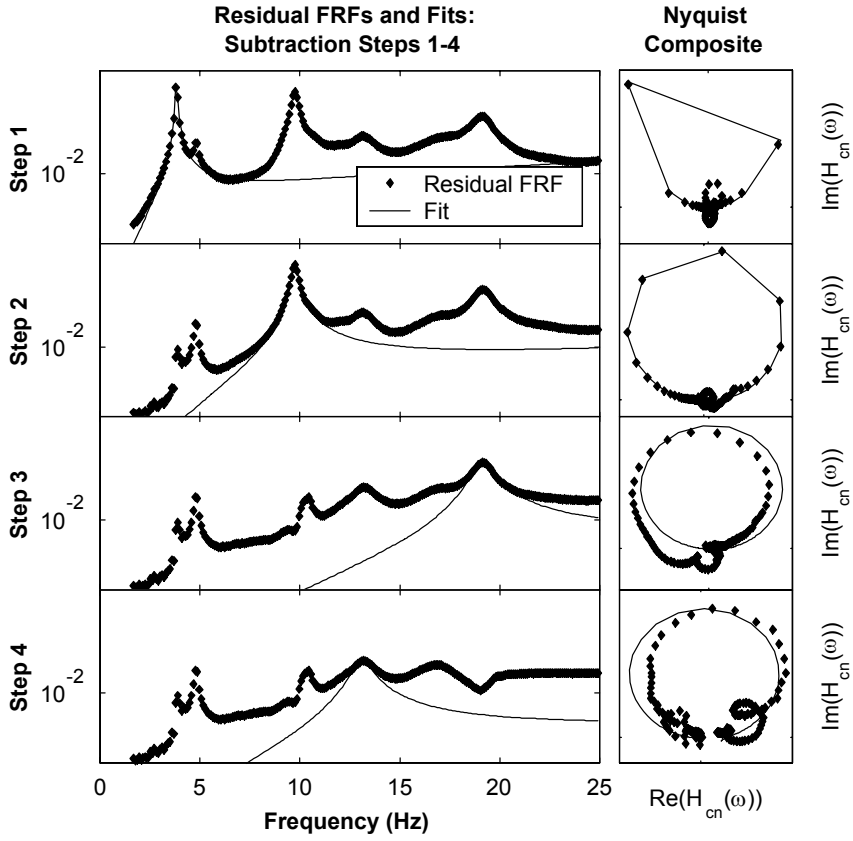

Figure 7: AMI Subtraction steps 1-4 for Z24 Bridge Data. LEFT: Composite residual FRF (.) and fit (-). RIGHT: Nyquist composite plots of residual FRF data (.) and fit (-).

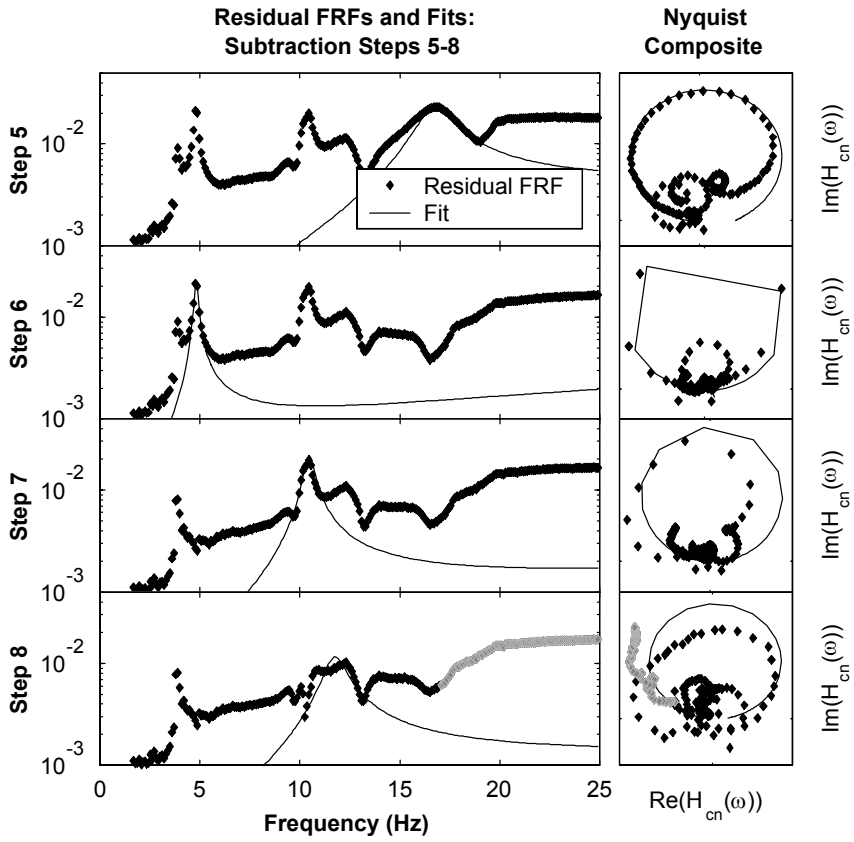

Figure 8: AMI Subtraction steps 5-8 for Z24 Bridge Data. LEFT: Composite residual FRF (.) and fit (-). RIGHT: Nyquist composite plots of residual FRF data (.) and fit (-). Data shown in gray in bottom pane was ignored in step eight.

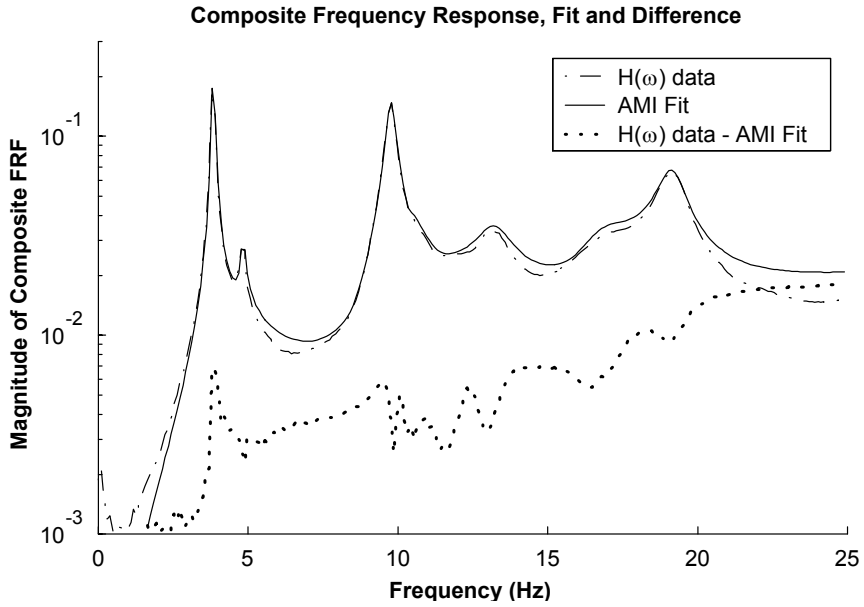

Figure 9: AMI results for Z24 bridge. Composite magnitude FRFs of data (.), AMI reconstruction (-) and the difference (-.).

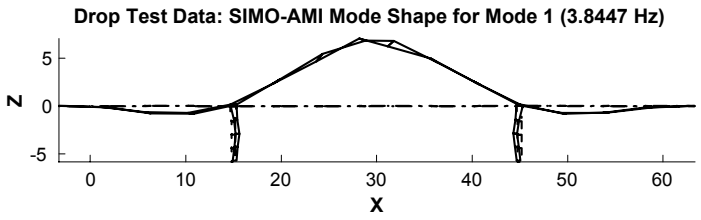

Figure 10: SIMO-AMI mode shape of Mode 1.

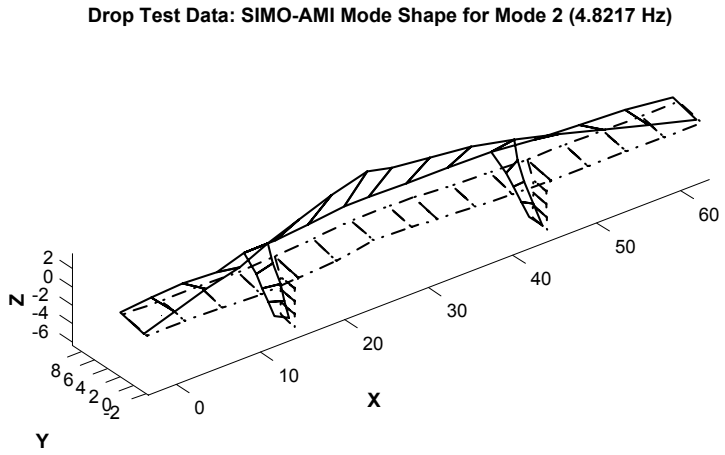

Figure 11: SIMO-AMI mode shape of Mode 2.

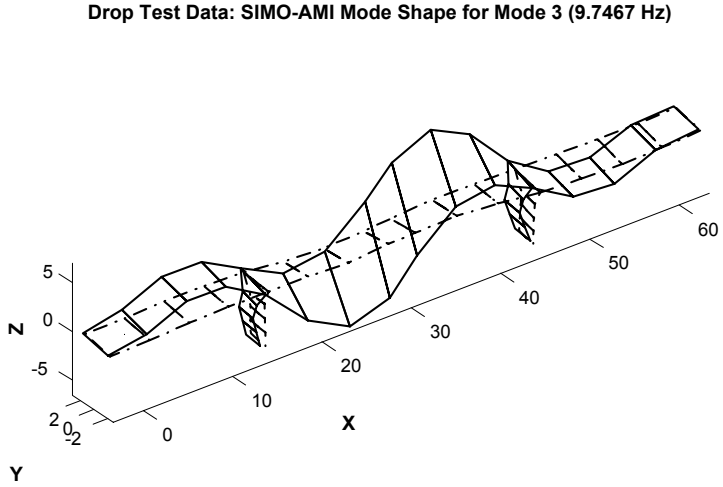

Figure 12: SIMO-AMI mode shape of Mode 3.

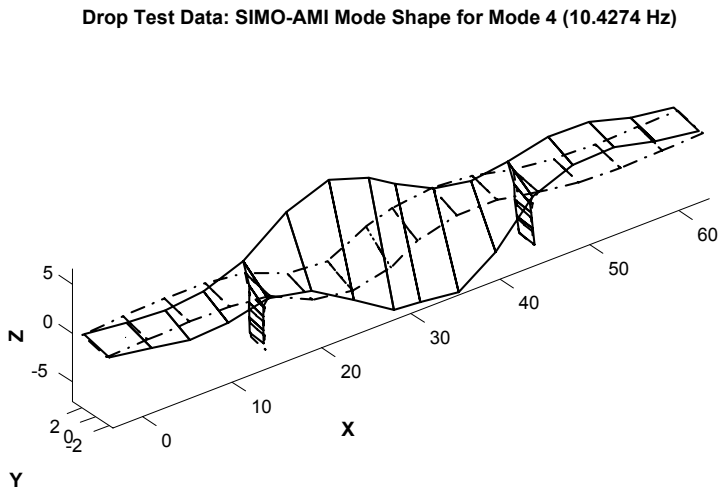

Figure 13: SIMO-AMI mode shape of Mode 4.

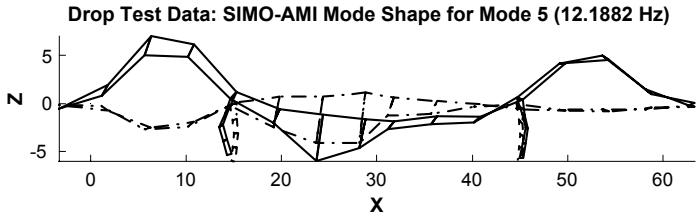

Figure 14: SIMO-AMI mode shape of Mode 5.

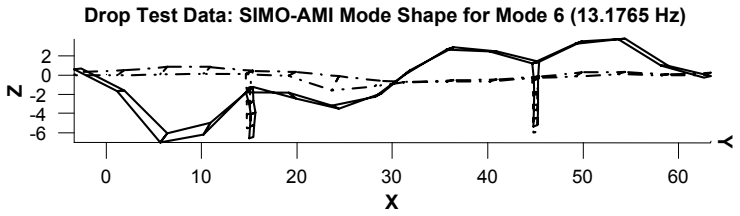

Figure 15: SIMO-AMI mode shape of Mode 6.

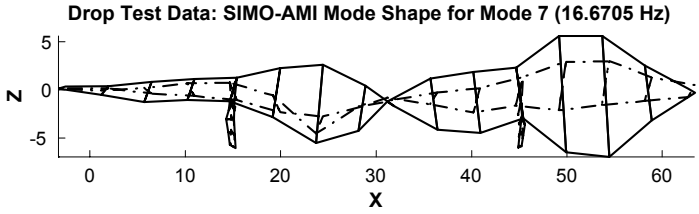

Figure 16: SIMO-AMI mode shape of Mode 7.

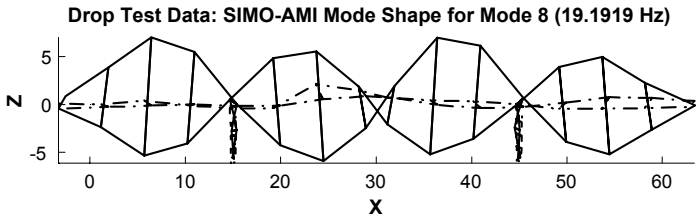

Figure 17: SIMO-AMI mode shape of Mode 8.